

Soft X-ray emissions of highly charged Si VII–Si XII in cool star—Procyon

G. Y. Liang^{*} and G. Zhao^{*}

National Astronomical Observatories, Chinese Academy of Sciences, Beijing 100012, P. R. China

Received date / Accepted date

ABSTRACT

Different observation data for cool star—Procyon (Obs.IDs of 63, 1461 and 1224) available from *Chandra Data Public Archive* were co-added and analyzed. Emissivities of emission lines of highly charged silicon ions (Si VII–Si XII) were calculated over temperatures by adopting the published data of Liang et al. (2007, *Atom. Data and Nucl. Data Tables*, **93**, 375). Using the emission measure derived by Raassen et al. (2002, *A&A*, **389**, 228), the theoretical line fluxes are predicted, and the theoretical spectra are constructed by assuming the Gaussian profile with instrumental broadening (0.06 Å). By detailed comparison between observation and predictions, several emissions lines are identified firstly such as emissions at 43.663 Å (Si XI), 45.550 Å (Si XII), 46.179 Å (Si VIII), 50.874 Å (Si X), 64.668 Å (Si IX), and 73.189 Å (Si VII) etc. Several emission lines are re-assigned in this work, such as the emission line at 52.594 Å to Si X (52.612 Å), at 69.641 Å to the blending of Si VII (69.632 Å) and Si VIII (69.664 Å) lines, as well as at 70.050 Å to Si VII (70.027 Å). The prediction reveals the large discrepancies between the *3s–2p* line (63.715 Å) *versus* *3d–2p* line (61.012 Å) again for lower charge stage Si VIII. Solar flare observation is also added for the assessment of present calculation. Different assignments for some lines between Procyon and solar flare, have been found to be due to the hotter emitter in Sun than in Procyon coronae.

Key words: line : identification – method : analytical – stars : coronae – X-rays : general

1 INTRODUCTION

Since the launch of *Chandra* and *XMM-Newton* X-ray missions, a large quantity of high quality X-ray spectra with high-resolution has been obtained for nearly all classes of astrophysical X-ray sources (Brinkman et al. 2000; Canizares et al., 2000; Audard et al. 2001; Brinkman et al. 2001; Ness et al. 2001; Rasmussen et al. 2001; Flanagan et al. 2004), which allows detailed plasma diagnostics to be performed for a wide range of celestial objects.

In the spectra of cool stars, rich emission lines of highly charged iron ions were detected due to its high abundance and high effective collecting area (200 cm² at 8.5 Å for HEG/MEG+ACIS-S instrument; 35 cm² at 10.0 Å for LETG+HRC-S instrument¹) between 6–18 Å. In this wavelength region, a good agree-

ment between predictions and observations is achieved so far (Behar et al. 2001), which profits from the Iron-Project (Hummer et al. 1993) and earlier running program—Opacity project (Seaton et al. 1994). Moreover, many laboratory experiments have been performed for iron by adopting grating and crystal spectrometers with high-resolution. The laboratory platform can be early vacuum spark, tokamak used for magnetic confinement fusion study, intense laser used for inertial confinement fusion research, and newly developed facility—electron beam ion trap (EBIT, Beiersdorfer 2003). Though the difference of *3s–2p* line intensity *versus* *3d–2p* line intensity of Fe XVII is a debating problem, a good theoretical performance is obtained when compared with spectra of highly charged sulfur and argon, as revealed by experimental measurements at Livermore EBIT (Lepson et al. 2003; Lepson et al. 2005a).

Besides rich emission lines of highly charged Fe ions, some emission lines of L-shell calcium, argon, sulfur and silicon have been identified for cool stars. Yet detailed analysis for spectra of these ions receive a scant attention due to the low effective area over the wavelength range of

^{*} Corresponding author: G.Y. Liang (gyliang@bao.ac.cn); G. Zhao (gzhaoh@bao.ac.cn)

¹ <http://cxc.harvard.edu/ciao/manuals.html>

35–100 Å spanned by lines of L-shell Si, Ar and Ca ions, and the absence of accurate atomic data of these ions. Several literatures (Keenan et al. 1998; Doyle et al., 1999; Keenan et al. 2000; Liang & Zhao 2006a; Liang et al. 2006c) also reveal the great potentials of L-shell silicon ions. Such as, the line intensity ratio $I(50.524)/I(50.691)$ of Si X, $I(52.306)/I(46.391)$ of Si XI are good diagnostic methods for the electron density; the line ratio $I(52.306)/I(43.743)$ of Si XI shows a good performance for the electron temperature (T_e) determination. Similar characteristics were explored for S X, Ar XIV and Ca XVI etc. (Keenan et al., 1993; 2000; 2001; 2003). Furthermore, spatial information of coronae could be assessed indirectly using correlation ($EM = n_e^2 V$) of the electron density with emission measure.

A laboratory measurement for silicon has been performed at the Livermore EBIT-II. Unfortunately, only the spectra between 80–90 Å is shown (Lepson et al. 2005b), yet it is enough to demonstrate the large differences between the measurement and theory. Recently, accurate atomic data including energy levels and spontaneous radiative decay rates were calculated for Si IX–Si XI by consideration of large configuration interaction and relativistic effects (Liang et al. 2007a). A self-consistent electron impact excitation rates over a large temperature grids are available, which are based on relativistic distort-wave (RDW) method. A laboratory measurement of soft X-ray spectra (40–180 Å) of highly charge silicon ions were also performed by irradiating the silicon target by intense laser beam at Institute of Physics, Chinese Academy of Sciences, which satisfactorily benchmarks the theoretical modelling at high density (Liang et al. 2007b).

In this work, we calculate the line emissivities of highly charged silicon ions (Si VI–Si XII) by adopting new available and accurate atomic data. The available observation data for cool star–Procyon (Obs.IDs 63, 1461 and 1224) are co-added and analyzed. By detailed comparison between the predictions and the co-added spectrum. Emissions lines of highly charged silicon are investigated. The observation of solar flare is also summarized for the assessment of the calculation.

2 OBSERVATIONS AND DATA ANALYSES

Procyon (F5 IV–V) is a solar-like star at a distance of 3.5 pc with mass of $1.75M_\odot$ and radius of $2.1R_\odot$, which has been observed by every X-ray space missions such as *Chandra* and *XMM-Newton*, for calibration. From *Chandra* Public Data Archive², four observations for Procyon can be available, with one observed by HRC-I instrument and none grating. For other three observations, HRC-S instrument was used in combination with low energy transmission grating (LETG), which covers a wavelength range of 6–176 Å. The description of the data sets is listed in Table 1.

In this work, the reduction of the data sets uses *Sherpa* software package in CIAO, version 3.3, with the science threads for HRC-S/LETG observations. The three spectra (with Obs.IDs of 63, 1461 and 1224) are co-added with the

Table 1. Observation data with HRC-S/LETG instrument for Procyon from *Chandra* public data archive.

Seq. Num.	Obs_ID	Instr./ Grating	Exposure time (ks)	Start time
280174	1224	HRC – S/LETG	20.93	1999 – 11 – 08
280411	1461	HRC – S/LETG	70.25	1999 – 11 – 07
290032	63	HRC – S/LETG	70.15	1999 – 11 – 06

`add_grating_spectra` tool to improve the signal-to-noise ratio, which results in a spectrum with total exposure time of 159.5 ks after times of bad counts were excluded. Similarly, the associate auxiliary response files (ARFs) are averaged by this tool. Here, the positive and negative spectra are analyzed separately by consideration of the different chip gaps for the two diffraction orders. Figs. 1–3 [histogram curves] show the co-added spectra for positive and negative diffraction orders in wavelength range of 43–88 Å spanned by emission lines of highly charged silicon ions (Si VI–Si XII).

Line fluxes are determined by modelling the spectra locally with narrow Gaussian profiles and constant value representing background and (pseudo-)continuum emissions determined in line-free region. The observed line width is about 0.06 Å over the interested region, which is comparable with the broadening of instrument for point-like source. The fluxes have been obtained after correction for the effective area. In the fitting, 1σ uncertainty was adopted to determine the statistical errors for the line fluxes. Here, only the line fluxes of highly charged silicon ions are listed in Table 2. For comparison, the line fluxes from Raassen et al. (2002) are listed, which reveals a good agreement for most peaks, although different observations are used.

Additionally, solar observation data in this wavelength region are also listed for completeness. The wavelength and line intensity (in unit of photons·cm^{−2}s^{−1} arcsec^{−1}) are from work of Acton et al. (1985), whereas the line intensities being less than 10 photons cm^{−2}s^{−1} arcsec^{−1} have not been given.

3 THEORETICAL MODELS

Collisional-radiative (CR) models for highly charged Si VII–Si XII ions are constructed based on the accurate atomic data from work of Liang et al. (2007a) and their unpublished data. These data are generated with the Flexible Atomic Code (FAC) provided by Gu (2003). 878, 312, 560, 320 and 350 energy levels have been included in predictions of line emissivities of Si VII–Si XI, respectively. These levels belongs to not only singly excited configurations, but also some doubly excited configurations for accounting for configuration interaction as fully as possible. Some energy levels are replaced by available experimental values from the National Institute of Science and Technology (NIST) database³. For Si XII, 40 energy levels are available from Chianti database (Landi et al. 2006), and used here. All possible decay channels among above listed levels by E1, M1, E2 and M2 type transitions, have been included in the present model for each charge states.

² <http://cxc.harvard.edu/cda/>

³ http://physics.nist.gov/PhysRefData/ASD/levels_form.html

A self-consistent calculation of electron impact excitation has been performed for the five ions (Si VII–Si XI), which based on the RDW method (Gu 2003). These data has been assessed for Si IX–Si XI in our previous work (Liang et al. 2007a). For $\Delta n = 0$ transitions among levels of ground and lower excited configurations, the excitation data is replaced by available R -matrix data, which properly considers resonant effects in the threshold region. To our best knowledge, the R -matrix calculation is not available for Si VII. So present RDW calculation of electron impaction excitation is used for Si VII by further consideration of self-consistency. Bell et al. (2001) calculate the electron impact excitation by using *ab initio* R -matrix method for excitations among levels of ground configuration $1s^2 2s^2 2p^3$ of Si VIII. These data replaces our results in predictions of line emissivities. For Si IX, resonant effects among levels of ground configuration, have been considered in predictions of level populations by using the data of Aggarwal (1983). Zhang et al. (1994) performed R -matrix calculation for 105 transitions among the 15 fine-structure energy levels belongings to $2s^2 2p$, $2s 2p^2$ and $2p^3$ configurations of Si X. However, an error was noted by Keenan (2000), who re-calculated the electron impact excitation rates for the 105 transitions with the R -matrix method. These data is adopted here for Si X. R -matrix results for 29 independent transitions among 10 fine-structure energy levels belongings to $2s^2$, $2s 2p$ and $2p^2$ configurations of Si XI were presented by Berrington et al. (1985). These accurate data replace the RDW calculations in the predictions of level populations of each charge states.

4 RESULTS AND DISCUSSIONS

By adopting the atomic data described in above section, line emissivities of Si VII–Si XII are calculated at an electron density of $3.0 \times 10^8 \text{ cm}^{-3}$ and electron temperatures ranging 0.1–5 MK. The electron density is a typical value for cool star with lower activities as revealed by previous works (Ness et al. 2002; Liang & Zhao 2006a). The silicon abundance adopts solar photospheric value, while the ionization equilibrium uses the result of Mazzotta et al. (1998). Previous works have revealed that the emission measure ($EM = n_e n_H V$) of Procyon has a continuous distribution and mainly dominates around 1–3 MK [see Fig. 3 in Ref. Raassen et al. (2002)]. The theoretical line fluxes of highly charged silicon ions, are derived by combining the line emissivities and the emission measure. The predicted line fluxes are listed along with the observed values for comparison in Table 2. Furthermore, the theoretical line fluxes couple the effective area extracted from ARFs files, and are folded by Gaussian profiles with full-width at half-maximum (FWHM) of 0.06 Å representing the observed line width. Figs. 1–3 show the theoretical spectra by color curves for different charge states. In these figures, the positive and negative diffraction are analyzed, separately. For most strong emission lines, the theoretical calculations agree well with the observations within the statistical uncertainty.

In solar case, we calculate the line intensity at a higher electron density of $5.0 \times 10^9 \text{ cm}^{-3}$ and temperatures of peak fractions for each charge state in the ionization equilibrium (Mazzotta et al. 1998). Further the predictions are

scaled by solar values at 44.20 Å (Si XII), 46.40 Å (Si XI), 50.52 Å (Si X), 55.41 Å (Si IX), 61.09 Å (Si VIII) and 70.05 Å (Si VII) for each charge state, respectively. In the following, we discuss the calculation and comparison in sequence of charge states.

Si XII Three emission lines at 44.029, 44.183 and 45.694 Å were identified in work of Raassen et al. (2002). These lines are reproduced again in present prediction, and their intensities are slightly higher than the observations, yet are still within 1σ statistical error. The scaled theoretical line intensities are also in agreement with the solar observation as shown in Table 2. Furthermore, we notice an emission at 45.550 Å, its intensity agrees with the Procyon observation in the both diffractions, as shown in Fig. 1. So we assign the emission to the $3s^2 S_{1/2} - 2p^2 P_{1/2}$ transition with wavelength of 45.521 Å. For the stellar spectra, this assignment is the first time to our best knowledge. This assignment is confirmed in solar observation with higher resolution (0.02 Å).

Si XI The present prediction satisfactorily reproduces the emission lines at 43.753, 46.301, 46.407, 49.217 and 52.307 Å as illustrated in Table 2 and Fig. 1. Around the peak at 43.753 Å, a weak line with wavelength of 43.663 Å is predicted, which can explain the left-side wing of the emission at 43.753 Å. In solar flare observation, this line is clearly resolved with a wavelength of 43.65 Å. Yet it still has not been identified so far. For the emission line at 52.307 Å, the calculation agrees with the observed flux in both diffractions, as shown in Table 2 and Fig. 1. However, Acton et al. (1985) pointed that there is a contamination from Al XI line at 52.244 Å. Present prediction indicates that the contribution from Al XI line can be negligible for Procyon and solar.

The line ratios among these emission lines show powerful diagnostic potentials for the electron density and temperature as revealed in work of Liang & Zhao (2006a). For example, the intensity of 43.753 Å line is sensitive to the electron temperature, and increases relative to the intensity of the 52.307 Å line with increasing the electron temperature [see Fig. 2 in Ref. Liang & Zhao (2006a)]. The larger discrepancy ($\sim 50\%$) of this line between the prediction and solar value reveals the higher electron temperature in solar flare.

Si X The two strong emission lines at 50.525 and 50.692 Å show an excellent n_e -diagnostic potential for inactive cool stars as reported in our previous work (Liang et al. 2006b). They are satisfactorily reproduced at the electron density of $3.0 \times 10^8 \text{ cm}^{-3}$ and the EM distribution determined by Raassen et al. (2002). For the emission at 50.361 Å, Raassen et al. (2002) assigned it to Si X according to the line-list of Kelly database (Kelly 1987)⁴, whereas the database is based upon the high-density plasma such as laser plasma. Fortunately, present work also predicts the emission with wavelength of 50.333 Å, but it contributes about $\sim 48\%$ in both diffractions. This means that there is unknown contamination from other lines. In solar flare observation, Acton et al. (1985) assign the observed emission at 50.35 Å to Fe XVI line with wavelength of 50.350 Å. So the left contribution at

⁴ <http://cfa-www.harvard.edu/amp/ampdata/kelly/kelly.html>

Table 2. The wavelengths and line fluxes (in unit of 1.0×10^{-4} phot. $\text{cm}^{-2}\text{s}^{-1}$) of emission lines of Si VI–Si XII in Procyon. The column of RMS02 denotes the value from work of Raassen et al. (2002). Wavelengths (λ_{\odot}) and fluxes (F_{\odot}) in solar flare observation are from work of Acton et al. (1985). The flux with subscript of 3CIE denotes the predicted fluxes from the present emissivity and the 3-temperature model (Raassen et al. 2002) for the Procyon coronae. F_{\odot}^p denotes the predicted line intensities normalized by solar values at 44.20 Å (Si XII), 46.40 Å (Si XI), 50.52 Å (Si X), 55.41 Å (Si IX), 61.09 Å (Si VIII) and 70.05 Å (Si VII) lines for each charge state, respectively.

ID	λ_{-} (Å)	Flux $_{-}$	λ_{+} (Å)	Flux $_{+}$	RMA02	λ_{\odot}	F_{\odot}	Ions	This work			Transitions		
									λ (Å)	F_{3CIE}	F_{\odot}^p	Upper level	Lower level	
1	43.663	0.10(9)	43.656	0.11(7)		43.65	21	Si XI	43.683	0.08	7	2s3p	3P_1	$2s^2$ 1S_0
2	43.753	0.61(9)	43.731	0.55(7)	0.54(8)	43.75	90	Si XI	43.763	0.39	35	2s3p	1P_1	$2s^2$ 1S_0
3	44.029	0.49(8)	44.002	0.33(6)	0.43(8)	44.02	138	Si XII	44.019	0.43	125	3d	$^2D_{3/2}$	2p $^2P_{1/2}$
4	44.183	0.73(9)	44.131	0.60(7)	0.67(10)	44.16	224	Si XII	44.165	0.76	224	3d	$^2D_{5/2}$	2p $^2P_{3/2}$
5a	44.275	0.28(8)	44.193	0.64(7)	0.52(10)	44.20	292	Si IX	44.213	0.08	3	$2s^2 2p 4d$	3D_1	$2s^2 2p^2$ 3P_2
5b								Si IX	44.215	0.10	4	$2s^2 2p 4d$	3D_2	$2s^2 2p^2$ 3P_1
5c								Si IX	44.249	0.15	6	$2s^2 2p 4d$	3D_3	$2s^2 2p^2$ 3P_2
6	45.550	0.14(8)	45.490	0.12(6)		45.51	57	Si XII	45.521	0.22	67	3s	$^2S_{1/2}$	2p $^2P_{1/2}$
7	45.694	0.34(9)	45.664	0.22(7)	0.20(4)	45.68	109	Si XII	45.691	0.45	135	3s	$^2S_{1/2}$	2p $^2P_{3/2}$
8a	46.179	0.16(5)	46.110	0.25(6)				Si VIII	46.133	0.09	1	$2s^2 2p^2(^3P)5d$	$^4P_{3/2}$	$2s^2 2p^3$ $^4S_{3/2}$
8b								Si VIII	46.148	0.05	1	$2s^2 2p^2(^3P)5d$	$^4P_{5/2}$	$2s^2 2p^3$ $^4S_{3/2}$
9a	46.301	0.31(5)	46.272	0.31(6)	0.25(7)	46.30	55	Si XI	46.263	0.08	8	2s3d	3D_1	$2s^2 2p$ 3P_0
9b								Si XI	46.298	0.15	15	2s3d	3D_2	$2s^2 2p$ 3P_1
9c								Si XI	46.313	0.06	6	2s3d	3D_3	$2s^2 2p$ 3P_2
10	46.407	0.49(5)	46.366	0.42(6)	0.40(8)	46.40	50	Si XI	46.399	0.41	50	2s3d	1D_2	$2s^2 2p$ 1P_1
11	49.217	1.40(8)	49.190	1.27(6)	1.44(14)	49.22	118	Si XI	49.222	1.06	94	2s3d	$^2F_{7/2}$	$2s^2 2p^2$ $^2D_{5/2}$
12	49.700	0.22(7)	49.673	0.32(6)	0.29(7)	49.71	43	Si X	49.701	0.09	1	$2s^2 2p(^1P)3d$	$^4D_{7/2}$	$2s^2 2p^2$ $^4P_{5/2}$
13	50.361	0.42(10)	50.334	0.44(8)	0.51(8)	50.35	195	Si X	50.333	0.20	1	$2s^2 2p(^3P)3d$	$^2D_{3/2}$	$2s^2 2p^2$ $^2P_{1/2}$
14	50.525	1.61(10)	50.512	1.38(9)	1.68(15)	50.52	12	Si X	50.524	1.45	12	$2s^2 3d$	$^2D_{5/2}$	$2s^2 2p^2$ $^2P_{3/2}$
15a	50.692	1.43(10)	50.676	1.04(8)	1.30(14)	50.69	74	Si X	50.691	1.08	19	$2s^2 3d$	$^2D_{3/2}$	$2s^2 2p^2$ $^2P_{3/2}$
15b								Si X	50.703	0.29	2	$2s^2 3d$	$^4F_{3/2}$	$2s^2 2p^2$ $^4P_{1/2}$
16	50.874	0.23(9)	50.828	0.15(8)				Si X	50.824	0.20	0	$2s^2 2p(^3P)3d$	1S_0	$2s^2 2p$ 1P_1
17	52.307	0.87(7)	52.304	0.88(13)	0.75(11)	52.30	88	Si XI	52.298	0.94	85	2s3s	$^2F_{7/2}$	$2s^2 2p^2$ $^2D_{5/2}$
18	52.453	0.29(7)	52.473	0.40(11)		52.48	15	Si X	52.484	0.13	3	$2s^2 2p(^3P)3d$	$^2F_{5/2}$	$2s^2 2p^2$ $^2D_{3/2}$
19	52.594	0.30(7)			0.35(8)	52.61	40	Si X	52.612	0.33	3	$2s^2 2p(^3P)3d$	3P_0	$2s^2 2p^2$ 3P_1
20a			55.078	0.67(7)	0.68(15)	55.11	17	Si IX	55.094	0.15	6	$2s^2 2p 3d$	3P_1	$2s^2 2p^2$ 3P_2
20b								Si IX	55.116	0.34	14	$2s^2 2p 3d$	3P_2	$2s^2 2p^2$ 3P_1
21a			55.246	1.19(8)	0.88(25)	55.23	< 10	Si IX	55.234	0.31	13	$2s^2 2p 3d$	3P_3	$2s^2 2p^2$ 3P_2
21b						55.28	28	Si IX	55.272	0.51	21	$2s^2 2p 3d$	3D_1	$2s^2 2p^2$ 3P_1
22a			55.347	2.26(9)	2.14(27)	55.37	22	Si IX	55.356	0.97	39	$2s^2 2p 3d$	3D_2	$2s^2 2p^2$ 3P_2
22b								Si IX	55.383	0.20	8	$2s^2 2p 3d$	3D_3	$2s^2 2p^2$ 3P_1
22c						55.41	43	Si IX	55.401	1.06	43	$2s^2 2p 3d$	3P_0	$2s^2 2p^2$ 1D_2
23			56.017	0.56(20)	0.19(11)	56.04	20	Si IX	56.027	0.07	3	$2s^2 2p(^2S)3p$	$^2P_{3/2}$	$2s^2 2p^2$ $^2D_{5/2}$
24			57.196	0.25(7)		57.20	25	Si X	57.208	0.29	6	$2s^2 2p(^3P)3s$	$^2P_{3/2}$	$2s^2 2p^2$ $^2D_{3/2}$
25			57.309	0.35(8)		57.35	17	Si X	57.366	0.62	4	$2s^2 2p(^3P)3s$	$^4P_{1/2}$	$2s^2 2p^3$ $^4S_{3/2}$
26a	61.012	1.66(14)			1.41(25)	61.03	17	Si VIII	60.989	0.58	8	$2s^2 2p^2(^3P)3d$	$^4P_{3/2}$	$2s^2 2p^3$ $^4S_{3/2}$
26b								Si VIII	61.022	1.14	17	$2s^2 2p^2(^3P)3d$	$^4P_{5/2}$	$2s^2 2p^3$ $^4S_{3/2}$
27	61.090	1.53(14)			1.38(24)	61.09	24	Si VIII	61.032	1.65	24	$2s^2 2p^2(^3P)3d$	3P_1	$2s^2 2p^2$ 3P_2
28	61.611	0.79(13)			0.52(17)	61.61	18	Si IX	61.600	0.07	3	$2s^2 2p 3s$	3P_1	$2s^2 2p^2$ 3P_1
29	61.847	0.85(13)			0.67(11)	61.85	21	Si IX	61.844	0.08	3	$2s^2 2p 3s$	3P_2	$2s^2 2p^2$ 3P_2
30	61.937	0.89(13)	61.971	1.11(14)	0.55(17)	61.92	32	Si VIII	61.792	0.18	3	$2s^2 2p^2(^1D)3d$	$^2D_{5/2}$	$2s^2 2p^3$ $^2D_{3/2}$
31	63.715	0.91(15)	63.777	0.57(11)	0.58(11)	63.72	352	Si VIII	63.716	0.17	2	$2s^2 2p^2(^3P)3d$	$^2F_{7/2}$	$2s^2 2p^3$ $^2D_{5/2}$
32			64.668	0.27(7)				Si IX	64.815	0.19	8	$2s^2 2p^2(^4P)3s$	3P_2	$2s^2 2p^3$ 3D_3
33			64.767	0.27(7)				Si IX	64.964	0.40	16	$2s^2 2p^2(^4P)3s$	3P_1	$2s^2 2p^3$ 3D_2
34a	67.152	0.73(16)	67.143	0.56(25)	0.48(11)	67.15	17	Si IX	67.066	0.04	2	$2s^2 2p^2(^4P)3s$	3P_2	$2s^2 2p^3$ 3P_1
34b								Si IX	67.071	0.11	4	$2s^2 2p^2(^4P)3s$	3P_2	$2s^2 2p^3$ 3P_2
35a	67.259	0.83(16)	67.287	0.58(14)	0.87(18)	67.24	42	Si IX	67.222	0.07	3	$2s^2 2p^2(^2D)3s$	3D_1	$2s^2 2p^3$ 3P_1
35b								Si IX	67.224	0.10	4	$2s^2 2p^2(^2D)3s$	3D_1	$2s^2 2p^3$ 3P_0
35c								Si IX	67.227	0.10	4	$2s^2 2p^2(^2D)3s$	3D_1	$2s^2 2p^3$ 3P_2
36a	67.417	0.72(15)	67.369	0.39(12)	0.68(14)	67.38	41	Si VIII	67.478	0.20	3	$2s^2 2p^3(^5S)3d$	$^4D_{1/2}$	$2s^2 2p^4$ $^4P_{1/2}$
36b								Ne VIII	67.382			4p	$^2P_{3/2}$	2s $^2S_{1/2}$
37	68.132	0.41(7)						Si VII	68.148	0.38	39	$2s^2 2p^3(^2P)3d$	3D_3	$2s^2 2p^4$ 3P_2
38a	69.641	2.19(11)	69.694	2.31(14)	2.03(21)	69.65	256	Si VIII	69.632	0.70	10	$2s^2 2p^2(^3P)3s$	$^4P_{5/2}$	$2s^2 2p^3$ $^4S_{3/2}$
38b								Si VII	69.664	0.46	47	$2s^2 2p^3(^2D)3d$	3P_2	$2s^2 2p^4$ 3P_2
39	69.797	1.22(11)	69.864	1.23(12)	1.05(14)	69.84	14	Si VIII	69.790	0.38	6	$2s^2 2p^2(^3P)3s$	$^4P_{3/2}$	$2s^2 2p^3$ $^4S_{3/2}$
40a	69.909	0.67(9)	69.993	0.73(12)		69.89	14	Si IX	69.896	0.46	19	$2s^2 2p 3p$	3D_3	$2s^2 2p^3$ 3D_2
40b								Si VIII	69.905	0.20	3	$2s^2 2p^2(^3P)3s$	$^4P_{1/2}$	$2s^2 2p^3$ $^4S_{3/2}$
41	70.050	0.80(9)	70.102	0.48(12)	0.70(11)	70.05	62	Si VII	70.027	0.61	62	$2s^2 2p^3(^2D)3d$	3D_3	$2s^2 2p^4$ 3P_2

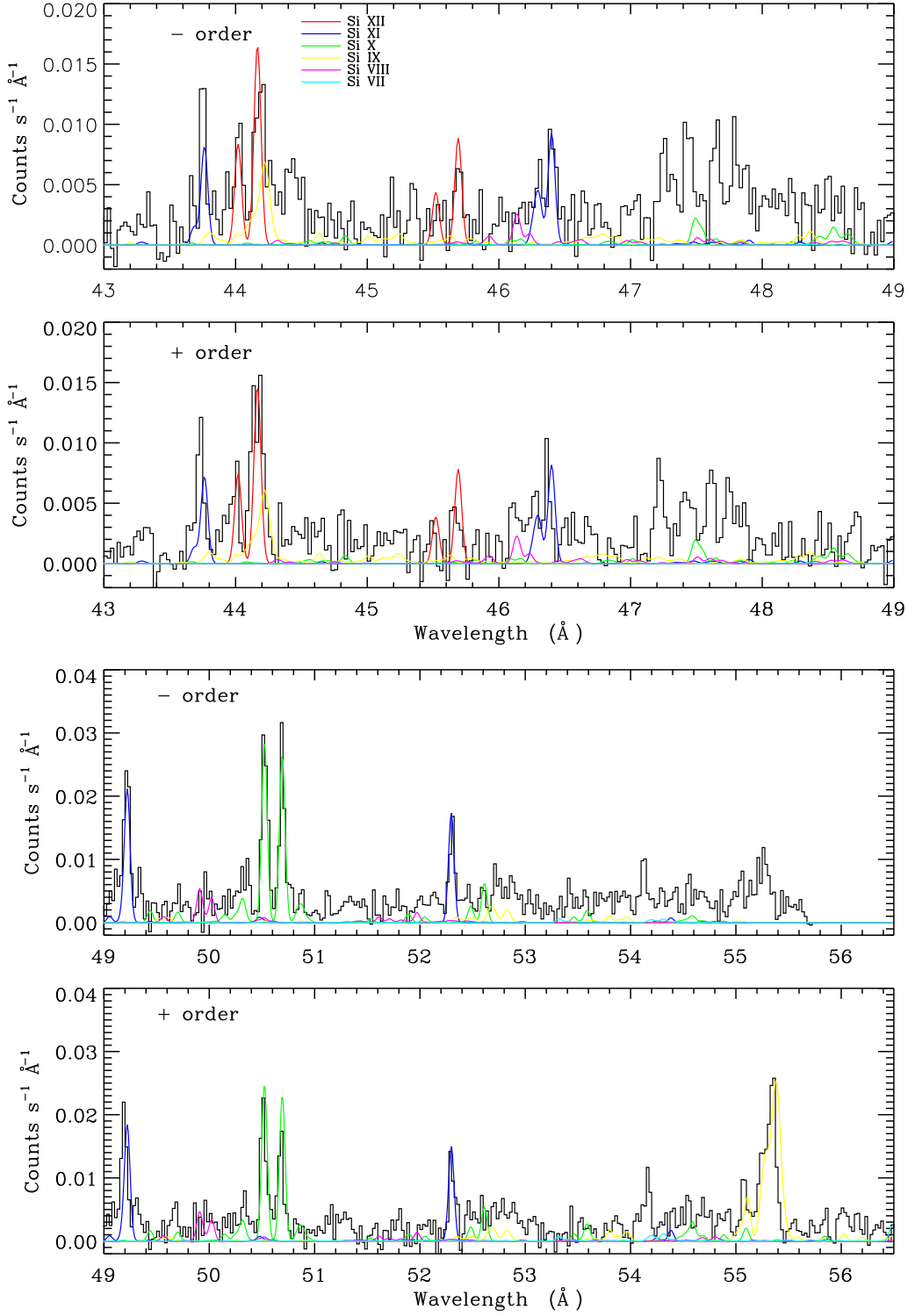


Figure 1. The co-added spectrum (with background extracted) of different observations (with Obs_IDs 63, 1461 and 1224) in wavelength range of 43–56 Å, is illustrated by histogram curves. The positive (*bottom*) and negative (*top*) panels are shown separately. The theoretical spectra of Si VII—Si XII are also overlapped with different colors. For clarity, the spectra in range of 43–88 Å is divided into five sections as shown in Figs. 2–3. (online color)

Table 2. —*Continued*

ID	λ_- (Å)	Flux $_-$	λ_+ (Å)	Flux $_+$	RMA02	λ_\odot	F_\odot	Ions	This work			Transitions		
									λ (Å)	F_{3CIE}	F_\odot^p	Upper level	Lower level	
42	72.443	0.36(15)	72.469	0.17(17)		72.41	19	Si VIII	72.421	0.15	2	$2s^2 2p^2(^3P)3s$	$^2P_{1/2}$	$2s^2 2p^3$ $^2D_{3/2}$
43	73.189	0.40(12)	73.124	0.50(22)				Si VII	73.123	0.64	65	$2s^2 2p^3(^4S)3d$	3D_3	$2s^2 2p^4$ 3P_2
44	76.010	0.90(18)	76.038	0.56(18)	0.77(13)	76.03	55	Si VIII	75.988	0.71	10	$2s^2 2p^3(^5S)3s$	$^4S_{3/2}$	$2s^2 2p^4$ $^4P_{5/2}$
45	76.157	0.25(15)	76.186	0.71(18)		76.16	21	Si VIII	76.196	0.46	7	$2s^2 2p^3(^5S)3s$	$^4S_{3/2}$	$2s^2 2p^4$ $^4P_{3/2}$

50.361 Å maybe from the Fe XVI in Procyon coroneae. However, In solar flare, the prediction reveals that the contribution from Si X at 50.35 Å of spectrum can be negligible. For peaks at 50.874 and 52.594 Å, the predicted line fluxes from the $2s2p(^3P)3d$ $^4F_{3/2}-2s2p^2$ $^4P_{1/2}$ (50.824 Å) and $2s2p(^3P)3d$ $^2F_{5/2}-2s2p^2$ $^2D_{3/2}$ (52.612 Å) transitions are comparable with the observed values within 1σ error, which indicates the contamination from Ni XVIII as revealed by Raassen et al. (2002) is negligible. But, in solar flare, the contribution from Ni XVIII is dominant, because Si X contributes only $\sim 8\%$. The present calculation predicts another emission lines at 52.484 Å. Moreover its intensity is 33% and 43% when compared to the observed flux in negative and positive diffractions, respectively. In solar flare, the contribution from Si X is less than 7% at 52.48 Å that is the emission line is still an unknown line. At the emission of 49.700 Å, the contribution from Si X (49.701 Å) is predicted to be $\sim 36\%$ and 2%, in Procyon and Sun, respectively.

In wavelength range of 57.0–57.5 Å, two emission lines ($\lambda=57.196$ and 57.309 Å) are detected in the positive spectrum, whereas they haven't been identified so far. In negative order spectrum, there are no counts between 55.7–58.5 Å, because of the chip gap. Present work predicts line flux at wavelengths of 57.208 Å being consistent with the observed values at 57.196, while the flux at 57.366 being higher than observed value at 57.309 Å by 75%. So we tentatively assign the two emission lines to the $2s2p(^3P)3s$ $^2P_{3/2}-2s2p^2$ $^2D_{5/2}$ and $2s2p(^3P)3s$ $^2P_{1/2}-2s2p^2$ $^2D_{3/2}$ transitions of Si X. In solar flare, 24% contribution of Si X is predicted for the two emissions.

Si IX Present calculation satisfactorily reproduces the line emissions at 55.246 and 55.347 Å. The line intensity ratio between them is sensitive to the electron density (n_e), whereas insensitive to the electron temperature (T_e) with variation less than 3% over $\log T_e$ (K)=5.9–6.3 [see Fig. 3 in Ref. Liang & Zhao (2007)]. The contribution of Si IX to the observed flux at 55.078 Å occupies a considerable part. When 14% contribution from Si X is considered, the contamination from Mg IX pointed out by Raassen et al. (2002) can be negligible. At the peak at 56.017 Å, we found the contribution from Si IX is very small. The major component maybe from S IX (56.081 Å) and Ni XIII (56.000 Å) as pointed out by Raassen et al. (2002). In solar flare, the contribution from Si IX (56.027 Å) is similarly very small ($\sim 15\%$). At the position about 44.218 Å, a large difference is found between the both diffractions, which is due to the low statistical performance in the interested wavelength region. The contribution from Si IX is estimated to be $\sim 100\%$ and 50% in the negative and positive diffractions, respectively. Additionally, contamination from second-order diffraction of O VII line (2×22.0975 Å) may be the origin of the difference, as pointed out by Acton et al. (1985) in the observation of solar flare.

The two $3s-2p$ transition lines at 61.611 and 61.847 Å are underestimated greatly in Procyon and solar flare. The large discrepancies compared with the $3d-2p$ lines at 55.359 Å, maybe from other unknown contamination. Indirect processes for populations on $3s$ and $3d$ levels and opacity effects also maybe the reasons of the deviations as in the debated case of Fe XVII (Ness et al. 2001; Beiersdorfer et al. 2004, ect.). The theoretical calculation also predicts an considerable line fluxes at 64.815 and 64.964 Å being from $2s2p^2(^4P)3s$ $^3P_2-2s2p^3$ 3D_3 and $2s2p^2(^2D)3s$ $^3P_1-2s2p^3$ 3D_2 transitions. But, no emission lines are detected at the two positions. We notice that the predicted fluxes agree with the observed values at measured wavelength of 64.668 and 64.767 Å. So we tentatively assign the two emission lines from $3s-2p$ transitions of Si IX by consideration of the 1% uncertainty of level energies for double excited levels.

Though the lines at 67.152 and 67.259 Å were assigned to be Mg IX (67.132 Å) and Ne VIII (67.350 Å), respectively, by Raassen et al. (2002), we also notice the contamination ($\sim 20-40\%$) from Si IX in Procyon and solar flare. The contribution of Si IX (69.896 Å) is up to $\sim 70\%$ at the peak of 69.909 Å as shown in Fig. 2. The left contribution is from Si VIII (69.905 Å). In solar flare, the contribution from Si VIII is predicted to be less than 20%.

Si VIII The line ratio between $3d-2p$ (61.022 Å) and $3s-2p$ (69.646 Å) lines is predicted higher than observation again as revealed in Si IX (Liang & Zhao 2007) and Fe XVII (Doron & Behar 2002, and references therein). The predicted line fluxes at 61.012 and 61.090 Å are slightly overestimated, but agree with observations within 1σ error for Procyon and solar flare observations. This reveals that the contamination from Mg IX (61.088 Å) can be negligible. At peaks of 69.641 and 69.797 Å, the contribution from $3s-2p$ transition of Si VIII is about 32%. Table 2 indicates that the line intensity of Si VII line (69.664 Å) is $\sim 65\%$ relative to the intensity of Si VIII line (69.632 Å). The total contribution from Si VIII (69.632 Å) and Si VII (69.664 Å) are predicted to be $\sim 50\%$ and $\sim 25\%$ for Procyon and solar flare, that is there is an unknown contamination besides the minor contribution of Fe XIV as reported by Acton et al. (1985).

We also notice that the prediction at 75.988 and 76.196 Å agree well with the observed fluxes at 76.010 and 76.157 Å. When a deviation of 1% in the double excited energy levels is considered, we tentatively assign the two emissions to Si VIII lines with wavelengths of 75.988 and 76.196 Å. In solar flare, the contribution from Si VIII is estimated to be $\sim 20-40\%$. Acton et al. (1985) assign the two emission lines to Fe XIV (76.023 Å) and Fe XIII (76.152 Å), respectively. Moreover, 10 photons \cdot cm $^{-2}$ s $^{-1}$ arcsec $^{-1}$ at 68.85 Å is detected in solar flare, which was assigned to the $2p^2 3s$ $^4P_{3/2}-2p^3$ $^4S_{3/2}$ transition of Si VIII with wave-

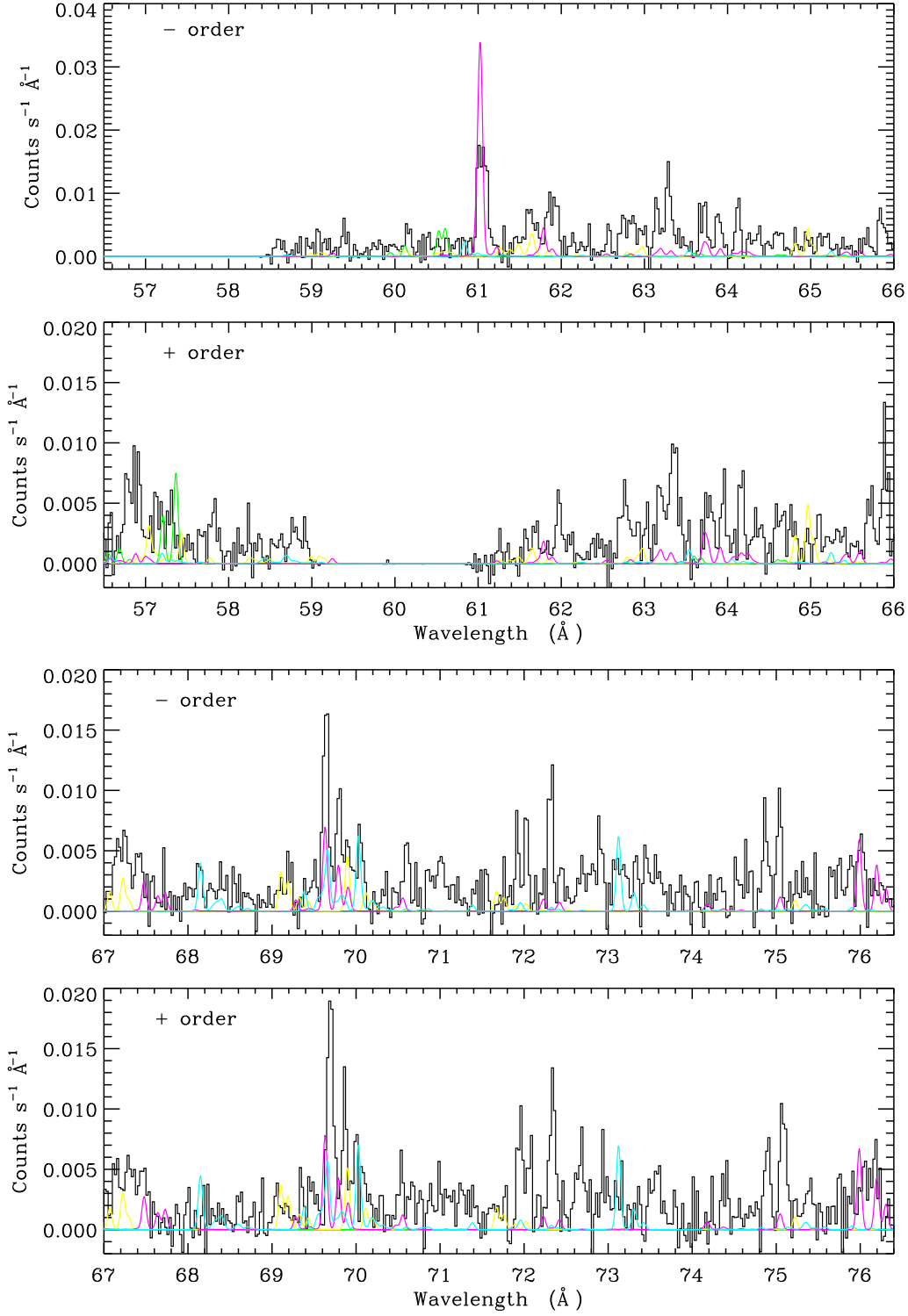


Figure 2. The co-added spectrum with background extracted in wavelength range of 56.5–76.4 Å. The description can refer to the caption of Fig. 1. (online color)

length of 68.853 Å by Acton et al. (1985). Yet, no dominant flux of Si VIII is predicted at this wavelength region. The lower contributions from Si VIII for solar flare, is due to the solar flare is hotter than Procyon coroneae.

Si VII As illustrated in Fig. 3 and Table 2, the

line flux of Si VII (70.027 Å) occupies about nearly 80%, that is the contribution from Fe XII (70.010 Å) and Fe XV (70.054 Å) is very small. Moreover, in the positive spectrum, the observed wavelengths around this region systematically longer than calculations and the observed values in the neg-

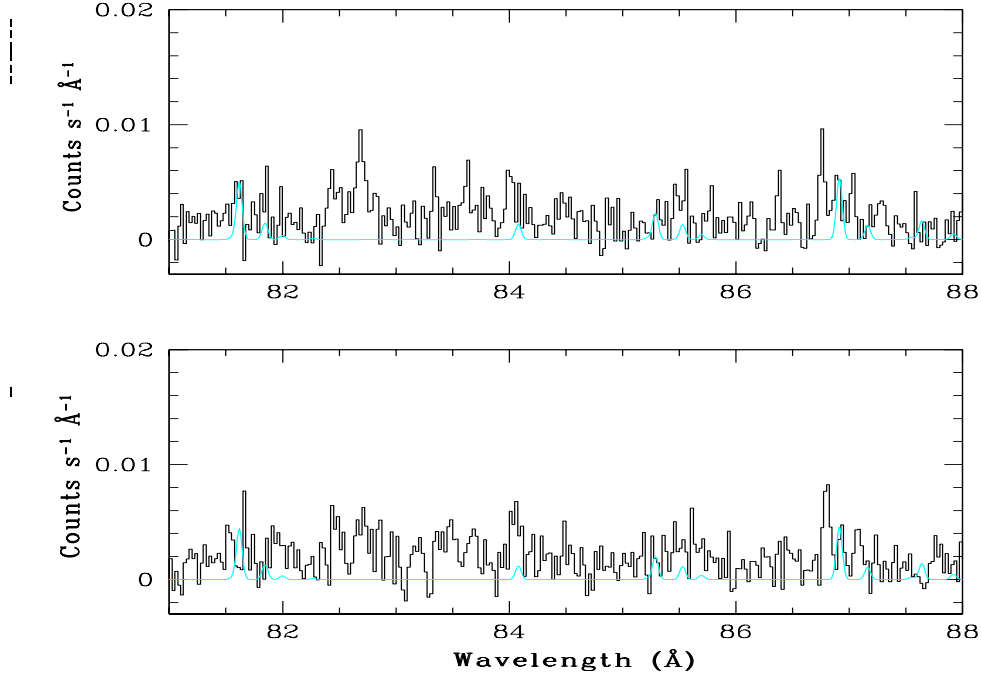


Figure 3. The co-added spectrum with background extracted in wavelength range of 81–88 Å. The description can refer to the caption of Fig. 1. (online color)

ative spectrum by ~ 0.06 Å. In solar flare, the contribution from Fe XV become strong as the assignment by Acton et al. (1985). At the peak around 68.132 Å of the negative spectrum of Procyon, the predicted intensity agrees well with observed value. So we tentatively assign the emission line to $2s^2 2p^3(^2P)3d\ ^3D_3-2s^2 2p^4\ ^3P_2$ transition (68.148 Å) of Si VII. This assignment is the first identification for stellar coronal spectra.

At peaks of 73.189, 81.61 and 86.876 Å, the calculation satisfactorily reproduces the Procyon observations. However, the former two lines haven't been identified so far, and the last emission line is assigned to Mg VIII by according to the line-lists of Kelly database. In the low-density astrophysical plasma, the contribution from Mg VIII can be negligible. At the peak of 81.61 Å in the positive spectrum, the observed wavelength is shorter than that in negative spectrum and the calculation by ~ 0.06 Å. This maybe due to the wavelength calibration in the positive diffraction.

5 CONCLUSION

In summary, available observation data (Obs.IDs of 63, 1461 and 1224) for cool star-Procyon are co-added and analyzed. By adopting our published atomic data and some unpublished data, line emissivities of Si VI–Si XII ions are calculated at an electron density of $3.0 \times 10^8 \text{ cm}^{-3}$ (typical value for cool stars) and temperatures over 0.1–5.0 MK. In this work, energy levels of 878, 312, 560, 320, 350 and 40 have been included for Si VII–Si XII, respectively. Moreover, decay rates of transitions (including E1, M1, E2 and M2) up to tens of thousand are included. Some electron impact exci-

tation data are replaced by available *R*-matrix data to take resonant effects into account as far as possible.

Based upon the EM derived by Raassen et al. (2002) and the calculated emissivities, we estimated the theoretical line fluxes of highly charged Si VII–Si XII ions. By detailed comparison between the observations and predictions, several emissions lines [with bold font in second or forth column of Table 2] are identified firstly to our best knowledge. The identification is assessed by comparing with solar spectrum with higher resolution (0.02 Å). The prediction indicates the large discrepancies between the $3s-2p$ line (69.641 Å) *versus* $3d-2p$ line (61.012 Å) again for lower charge stage Si VIII. This reveals that more accurate calculation of cross section in electron-ion interactions is very necessary. For emission lines at 52.594 Å (Si X), 55.078 Å (Si IX) and 70.027 Å (Si VII), this work indicates that the contamination from Ni XVIII (52.615 Å), Mg IX (55.060 Å) and Fe XII (70.010 and 70.054 Å of Fe XV), respectively, can be negligible for Procyon. However, in solar flare, the contaminations from Mg, Fe and Ni ions become dominant. This is due to the solar flare is hotter than the Procyon coronae. For the peak around 69.641 Å, Si VII line has the comparable contribution with the Si VIII lines identified by Raassen et al. (2002). However, their total contribution is less than 25% in solar flare. The discrepancies and the identification strongly suggest the benchmark from laboratory measurements at low-density plasmas.

ACKNOWLEDGMENTS

This work was supported by the National Natural Science Foundation of China under grant Nos. 10603007 and

10521001, as well as National Basic Research Program of China (973 Program) under grant No. 2007CB815103.

REFERENCES

- Acton L.W., Bruner M.E., Brown W.A., et al., 1985, ApJ, 291, 865
- Aggarwal K.M., 1983, J. Phys. B, 16, L59
- Audard M., Behar E., Güdel M., et al., 2001, A&A, 365, L329
- Behar E., Cottam J., Kahn S. M., et al., 2001, ApJ, 548, 966
- Beiersdorfer P., 2003, Annu. Rev. Astron. Astrophys., 41, 343
- Beiersdorfer P., Bitter M., Von Goeler S., Hill K.W., 2004, ApJ, 610, 616
- Bell K.L., Matthews A., Ramsbottom C.A., 2001, MNRAS, 322, 779
- Berrington K.A., Burke P.G., Dufton P.L., Kingston A.E., 1985, Atom. Data and Nucl. Data Tables, 33, 195
- Brinkman A. C., Behar E., Güdel M., et al., 2001, A&A, 365, L324
- Brinkman A. C., Gunsing C. J. T., Kaastra J. S., et al., 2000, ApJ, 530, L111
- Canizares C. R., Huenemoerder D. P., Davis D. S., et al., 2000, ApJ, 539, L41
- Doron R., Behar E., 2002, ApJ, 574, 518
- Doyle J.G., Keenan F.P., Ryans R.S.I., et al., 1999, Solar Physics, 188, 73
- Flanagan K.A., Canizares C.R., Dewey D., et al., 2004, ApJ, 605, 230
- Gu M. F., 2003, ApJ, 582, 1241
- Hummer D.G., Berrington K.A., Eissner W., et al., 1993, A&A, 279, 298
- Keenan F.P., 2000, MNRAS, 315, 450
- Keenan F.P., Aggarwal K.M., Katsiyannis A. C., et al., 2003, Solar Physics, 217, 225
- Keenan F. P., Aggarwal K.M., Williams D. R., et al., 2001, MNRAS, 326, 1387
- Keenan F.P., Conlon E.S., Foster V.J., et al., 1993, Solar Physics, 145, 291
- Keenan F.P., O'Shea E., Thomas R.J., et al., 2000, MNRAS, 315, 450
- Keenan F.P., Pinfield D.J., Mathioudaskis M., et al., 2000, Solar Physics, 197, 253
- Keenan F.P., Pinfield D.J., Woods V.J., et al., 1998, ApJ, 503, 953
- Kelly R.L. 1987, J.Phys.Chem.Ref.Data, 16, Suppl. 1.
- Landi E., Del Zanna G., Young P.R., Dere K.P., Mason H.P., Landini M., 2006, ApJS, 162, 261
- Lepson J.K. Beiersdorfer P., Behar E., Kahn S.M., 2003, ApJ, 590, 604
- Lepson J.K. Beiersdorfer P., Behar E., Kahn S.M., 2005a, ApJ, 625, 1045
- Lepson J.K. Beiersdorfer P., Behar E., Kahn S.M., 2005b, Nucl. Inst. and Meth. in Phys. Research B, 235, 131
- Liang G.Y., Zhao G., 2006a, AJ, 132, 1547
- Liang G.Y., Zhao G., Shi J.R., 2006b, AJ, 132, 371
- Liang G.Y., Zhao G., Shi J.R., 2006c, MNRAS, 368, 196
- Liang G.Y., Zhao G., 2007, New Astronomy, 12, 435
- Liang G.Y., Zhao G., Zeng J.L., 2007, Atom. Data and Nucl. Data Tables, 93, 375
- Liang G.Y., Zhao G., Zhong J.Y., et al., 2007, ApJ (in re-review)
- Mazzotta P., Mazzitelli G., Colafrancesco S., Vittorio N., 1998, ApJS, 133, 403
- Ness J. -U., Mewe R., Schmitt J. H. M. M., et al., 2001, A&A, 367, 282
- Ness J. -U., Schmitt J. H. M. M., Audard M., Güdel M., Mewe R., 2003, A&A, 407, 347
- Ness J. -U., Schmitt J. H. M. M., Burwitz V., et al., 2002, A&A, 394, 911
- Raassen, A. J. J., Mewe, R., Audard, M., et al., 2002, A&A, 389, 228
- Rasmussen A. P., Behar E., Kahn S. M., et al., 2001, A&A, 365, L231
- Seaton M.J., Yan Y., Mihalas D., Pradhan A.K., 1994, MNRAS, 266, 805
- Zhang H.L., Graziani M., Pradhan A.K., 1994, A&A, 283, 319

This paper has been typeset from a \TeX / \LaTeX file prepared by the author.